Hindawi Publishing Corporation
Mathematical Problems in Engineering
Volume 2015, Article ID 485319, 12 pages
http://dx.doi.org/10.1155/2015/485319

Research Article

Effect of Cyclic Loading on the Lateral Behavior of Offshore Monopiles Using the Strain Wedge Model

Keunju Kim,[1] Boo Hyun Nam,[2] and Heejung Youn[1]

[1]*Department of Civil Engineering, Hongik University, Sangsu-dong 72-1, Mapo-gu, Seoul 04066, Republic of Korea*
[2]*Civil, Environmental, and Construction Engineering Department, University of Central Florida, Orlando, FL 32816, USA*

Correspondence should be addressed to Heejung Youn; geotech@hongik.ac.kr

Received 24 April 2015; Revised 28 July 2015; Accepted 13 August 2015

Academic Editor: Alessandro Palmeri

This paper presents the effect of cyclic loading on the lateral behavior of monopiles in terms of load-displacement curves, deflection curves, and p-y curves along the pile. A commercial software, Strain Wedge Model (SWM), was employed, simulating a 7.5 m in diameter and 60 m long steel monopile embedded into quartz sands. In order to account for the effect of cyclic loading, accumulated strains were calculated based on the results of drained cyclic triaxial compression tests, and the accumulated strains were combined with static strains representing input strains into the SWM. The input strains were estimated for different numbers of cycles ranging from 1 to 10^5 and 3 different cyclic lateral loads (25%, 50%, and 75% of static capacity). The lateral displacement at pile head was found to increase with increasing number of cycles and increasing cyclic lateral loads. In order to model these deformations resulting from cyclic loading, the initial stiffness of the p-y curves has to be significantly reduced.

1. Introduction

Monopiles have been frequently used to resist offshore environmental loads such as wind, wave, tidal, and ice loads. Unlike onshore loading conditions, the offshore environmental loads have two main differentiated characteristics; the magnitude of lateral load is significant and the load is cyclic. Cyclic loading may cause serious problems in offshore structures and surrounding soils depending on the soil type and properties. During the design lifetime, the offshore structure is known to undergo about 10^8 lateral cyclic loading events of varying amplitude [1]. During this great number of cycles, the offshore structures need to endure fatigue, and surrounding soils should not alter much to satisfy the lateral capacity and displacement criteria. Engineering properties of surrounding soils can deteriorate because of a possible accumulation of excess pore water pressure induced by cyclic loading. For cohesive soils, the deterioration of the clay structure or the forming of a gap between soil and pile could be the main concerns causing degradation of engineering properties. Furthermore, an excessive number of cycles may induce friction fatigue along the pile regardless of soil type, which is another critical factor causing the deterioration of side resistance. For cohesionless soils, the excess pore water pressure is unlikely to develop as the soils are normally in drained conditions; rather both the strength and stiffness will increase due to densification of surrounding soils. Still, the lateral displacement and rotation at pile head accumulate possibly leading to a serviceability problem. This is believed to be considerable especially in the case of a one way cyclic loading.

The p-y curves have been widely used in practice to analyze the lateral behavior of piles. Many p-y curves have been proposed chiefly considering soil types (sand or clay), loading types (static or cyclic), and ground water conditions (soil under water or above water). In conventional design process, the soils supporting piles are replaced by a set of nonlinear springs, and the pile is assumed to act as a beam supported by the springs. A soil spring acts as a reaction, p, per lateral displacement, y, at a pile elevation. The concept was first introduced by Winkler [2] and has been updated by many researchers. Reese et al. [3] suggested a parabola p-y

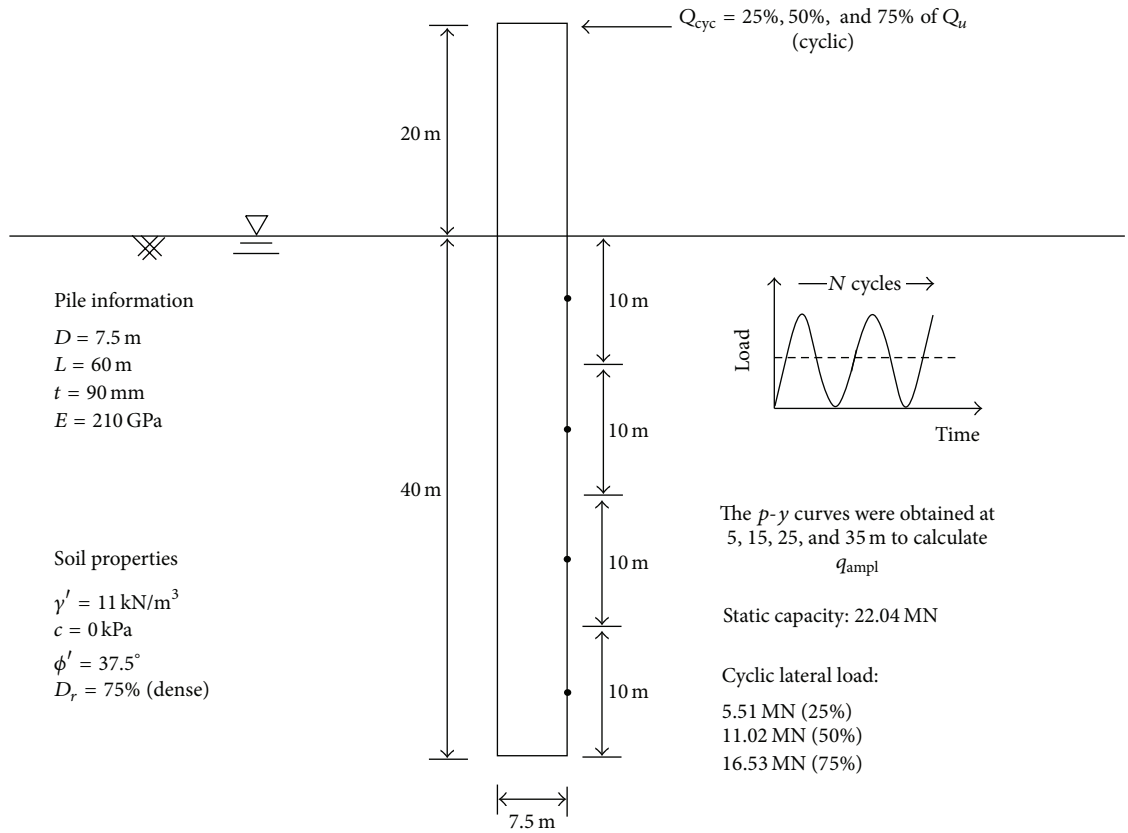

Figure 1: Material properties of soil and pile, and loading conditions.

curve and an empirical adjustment factor A with different definitions for static and cyclic loading. Later, simplified approaches to establish the p-y curves have been reported [4].

As the aforementioned p-y curves were developed not for offshore wind turbines but for offshore oil platforms, there have been concerns that the offshore monopiles with their large lateral load compared to dead weight may behave differently. Moreover, the available p-y curves are validated for small piles with diameter of 1-2 m under small number of cycles ($N < 100$) only, while offshore monopiles have 5–7 m diameter and are subject to much more cycles. The existing p-y curves may not be applicable to the offshore monopiles without appropriate validation. Achmus et al. [1] instead developed design charts for offshore wind turbine foundation installed in sandy soils based on a stiffness degradation model. Cyclic triaxial tests and series of numerical analyses were carried out in order to investigate the long-term behavior under cyclic loading. Wichtmann et al. [5, 6] suggested a High Cycle Accumulation (HCA) model, which captures the effect of cyclic loading, and performed series of finite element analyses. The proposed HCA model was based on series of drained cyclic triaxial compression and extension tests [7, 8]. Instead of using complicated FEM, practical software analysing the lateral behavior of a pile by means of the Strain Wedge Model (SWM) was applied in [9] to quantify the deformation of an offshore wind turbine, illustrating an increase in the lateral displacement with increasing number of cycles. Recently, nonlinear p-y curves in cohesive soils were proposed accounting for soil-pile interaction, degradation in soil stiffness and strength due to cyclic loading, soil-pile gap forming, and radiation damping [10].

The numerical analyses were often supported by small or full scale test results. Roesen et al. [11, 12] investigated the soil-pile interaction of a monopile embedded in sands using small scale tests. The monopile was subject to a high number of one way cyclic loads (up to 60,000 cycles) with varying amplitude, mean load, and loading period. It was reported that the increase of the accumulated rotation with growing number of cycles could be approximated by a power function. Moller and Christiansen [13] conducted small scale tests to evaluate the existing p-y methods for static and cyclic loading and compared them with numerical analysis results.

This paper investigates the lateral behavior of a monopile subjected to a lateral cyclic loading, focusing particularly on the influences of the number of cycles and magnitude of cyclic lateral load. The effect of cyclic loading was assessed in terms of accumulated strains, which were later modified into the input strains used in the SWM [14]. The load-displacement curves, deflection curves, and cyclic p-y curves were obtained from SWM; and the lateral behavior of the monopile was analyzed.

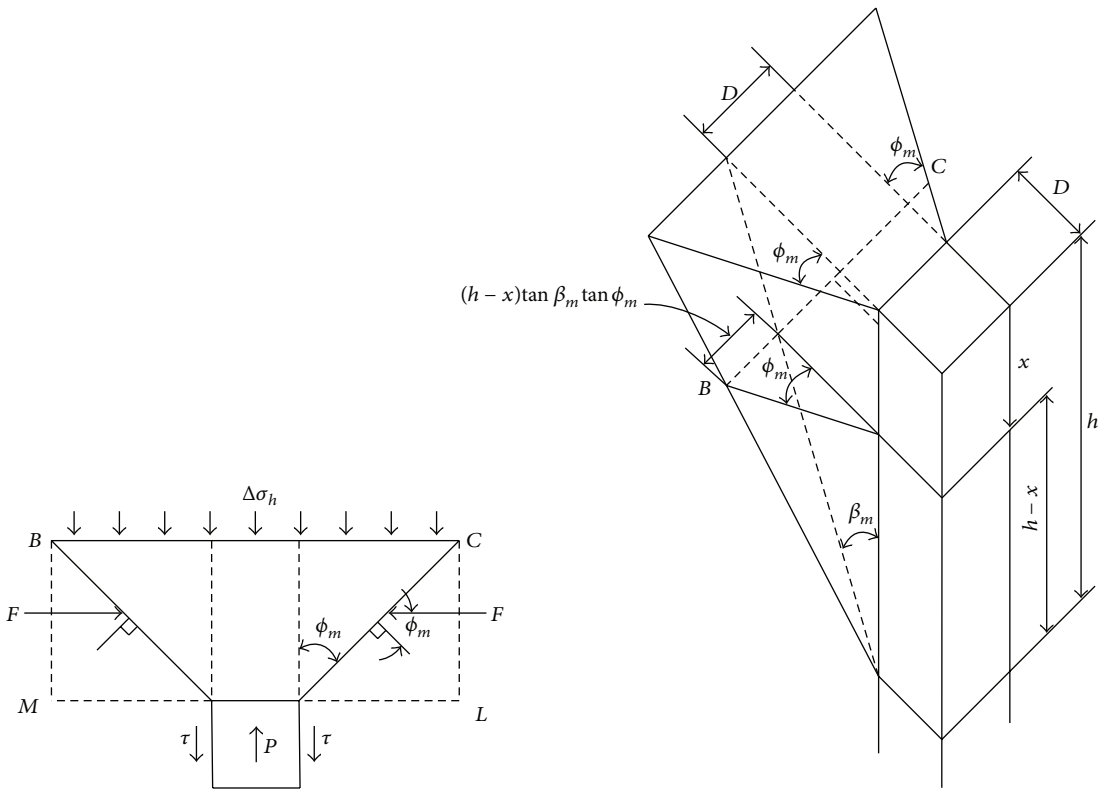

Figure 2: Basic strain wedge in uniform soil (redrawn from [17]).

2. Material Properties and Loading Conditions

Figure 1 illustrates the offshore monopile embedded in quartz sands used in this study along with the pile and soil properties. The monopile, which has to resist relatively large lateral load, was a 60 m long and 90 mm thick steel tube, the diameter of which was 7.5 m. The pile was assumed to be linear elastic with Young's modulus of 210 GPa; the soils were assumed to be homogeneous through the layer. The material properties of the soil were adopted from a previous research, which investigated the effect of cyclic loading on the accumulated displacement of pile embedded into quartz sand [1]. The investigated sands have a peak internal friction angle of 37.5°, effective unit weight of 11 kN/m^3, and a cohesion of 0 kPa. The used soil was dense; thus, the relative density of the soil was assumed to be 75% throughout the layer, and the maximum and minimum void ratio were assumed to be 0.874 and 0.577 as used in the literature [7].

The information of cyclic lateral load is difficult to quantify because the load is site specific and variable in direction and magnitude. Therefore, the static lateral capacity (Q_u) of the monopile was calculated using the load-displacement curve at seabed from the SWM analysis, and the cyclic lateral loads were chosen as 25%, 50%, and 75% of the static capacity. The static lateral capacity was determined to be 22.04 MN at 38.1 mm of lateral displacement at seabed [15]. Consequently, the used cyclic lateral loads, Q_{cyc}, were 5.51, 11.02, and 16.53 MN, respectively. In the simulations, after applying a certain number of cyclic loads, the pile head was loaded with the lateral load of 22.04 MN to obtain the load-displacement relationship at pile head, and the p-y curves were obtained at 5, 15, 25, and 35 m depth along the pile below seabed.

3. Input Parameter Calculation

3.1. SWM Analysis. The Strain Wedge Model was initially suggested by Norris [16] and has been used to predict the behavior of flexible piles under lateral loading. Figure 2 presents the configuration of the Strain Wedge Model in uniform soil. The soil resistance against lateral loading is developed by a 3-dimensional passive wedge of soil at the front of the pile, and the configuration of the passive wedge is determined by the mobilized friction angle and pile diameter: $\beta_m = 45° + \phi_m/2$, D is the pile diameter, h is the height of the passive wedge, $\Delta\sigma_h$ is the variation in horizontal stress at wedge face, and τ is the shear stress at pile side. The advantage of the SWM is the transfer of the stress-strain-strength behavior of soil observed in element tests to the 1-dimensional Beam on Elastic Foundation (BEF) parameters. While the conventional p-y curves were experimentally derived from strains developed along the laterally loaded pile, the SWM provides a theoretical link between soil properties and lateral behavior of pile. The horizontal strain (ε_h) in the passive wedge is used to determine the deflection of the pile (y), and the variation of horizontal stress at the passive wedge is used to determine the soil resistance (p) associated with the BEF.

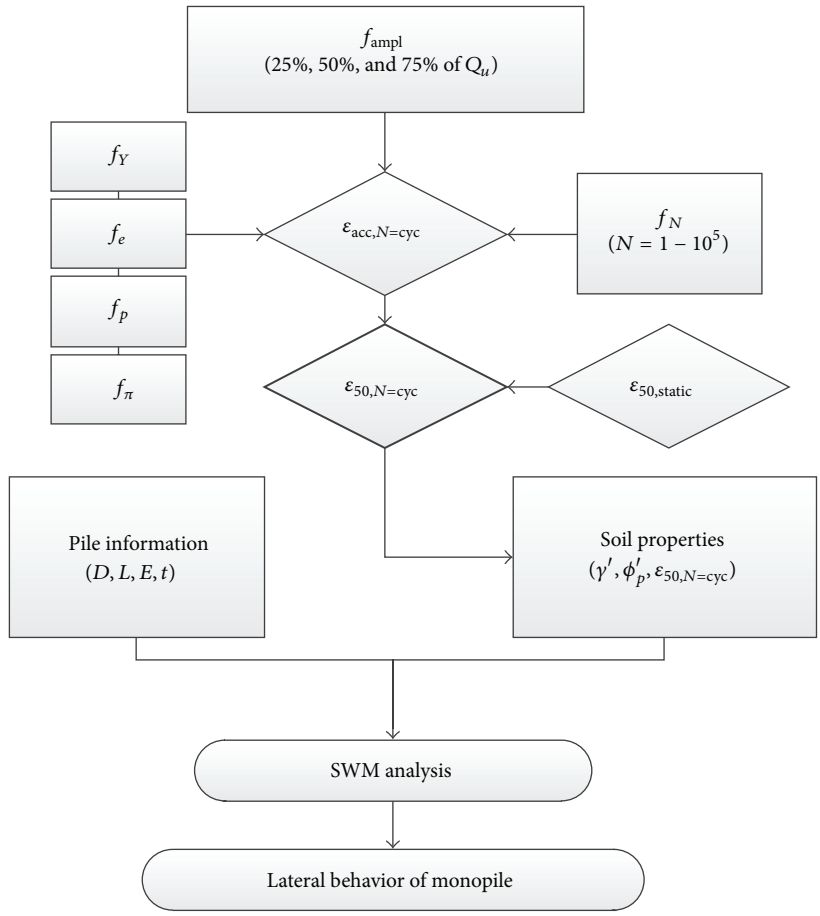

Figure 3: Flow chart of SWM analysis accounting for cyclic loading.

Details of the theory and the assumptions used in the SWM are provided, for example, in [17].

Figure 3 shows a flow chart illustrating the numerical process proposed in this paper to analyze the monopile under cyclic lateral loading. The key input parameters into the SWM include the static strain at 50% peak strength ($\varepsilon_{50,static}$), dimension and Young's modulus of the steel pile, and the material properties of the surrounding soils. The SWM requires the strain at 50% peak strength (ε_{50}) in order to assess the lateral behavior of the pile under the static loading condition. On the other hand, the strain under the cyclic loading condition accumulates as the number of cycles increases ($\varepsilon_{acc,N=cyc}$), which means the strain will not recover to the original state of the pile upon unloading [7]. Therefore, the strain under cyclic loading needs to be modified into an input strain ($\varepsilon_{50,N=cyc}$) considering key factors such as the magnitude of cyclic lateral loads, average mean stress, void ratio, and number of cyclic loads. The proposed methodology to assess the key factors will be presented in later sections.

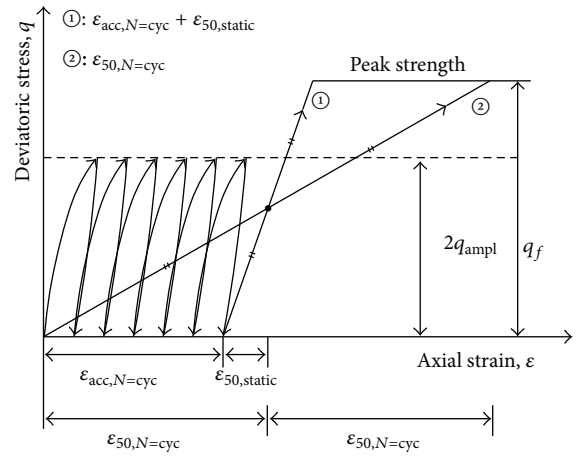

Figure 4: Accumulated strain after N cycles, and input strain in q-ε plane.

3.2. Input Strain under Cyclic Loading ($\varepsilon_{50,N=cyc}$). Figure 4 shows the concept of calculating the accumulated strain developed by the applied number of cycles in the q-ε plane. At the end of N cycles, the plastic strain has accumulated to some extent, which is denoted by $\varepsilon_{acc,N=cyc}$. During a subsequent monotonic loading, the deviatoric stress of the soil would start from the accumulated strain at zero deviatoric stress to peak strength (as shown by line ①).

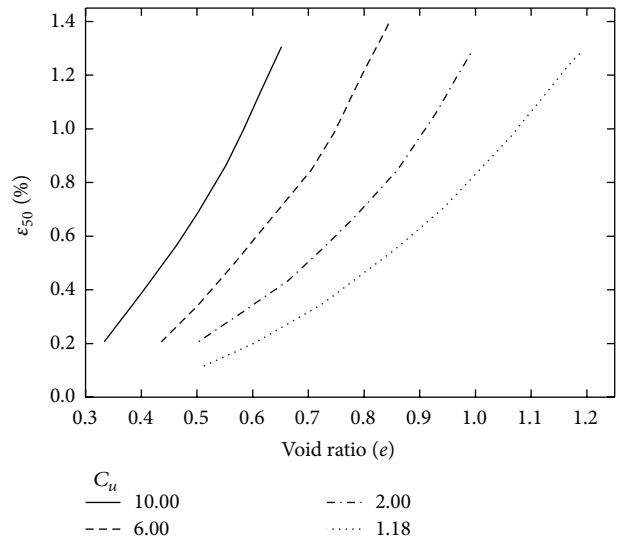

FIGURE 5: Relation between static strain ($\varepsilon_{50,\text{static}}$) and void ratio ($e$) for different C_u (redrawn from [16]).

The probable strain at failure after the considered number of cycles was calculated by summing twice the accumulated strain ($\varepsilon_{\text{acc},N=\text{cyc}}$) and twice the static strain at 50% peak strength ($\varepsilon_{50,\text{static}}$). Then the strain at failure under cyclic loading was modified into input strain at 50% peak strength ($\varepsilon_{50,N=\text{cyc}}$), which means the corresponding line for a monotonic loading incorporating the cumulative effects follows line ②. Even though this approach does not perfectly capture the real behavior of soils and the real accumulated strain, the calculation procedure seems to be simple and reasonable. The input strains used in this study were calculated by

$$\varepsilon_{50,N=\text{cyc}} = \varepsilon_{50,\text{static}} + \varepsilon_{\text{acc},N=\text{cyc}}. \tag{1}$$

The static strain ($\varepsilon_{50,\text{static}}$) varies with the void ratio (i.e., relative density) and coefficient of uniformity of the sand as shown in Figure 5. With the chosen relative density (75%) and coefficient of uniformity (1.8) from previous research [7], the static strain ($\varepsilon_{50,\text{static}}$) of the studied soil was calculated to be 0.42% at the reference confining pressure of 42.5 kPa. The static strain needs modification to account for the effect of confining pressure, which varies along the pile length. Thus, the static strain under the reference confining pressure (42.5 kPa) is modified into an input value for the effective overburden pressure at desired depth using (2) proposed in [16]. Consider the following:

$$\left(\varepsilon_{50}\right)_i = \left(\varepsilon_{50}\right)_{42.5} \left(\frac{\left(\overline{\sigma}_{v0}\right)_i}{42.5}\right)^{0.2}. \tag{2}$$

3.3. Accumulated Strain ($\varepsilon_{\text{acc},N=\text{cyc}}$). The accumulated strains as a result of a large number of cycles were calculated based on test data from cyclic drained triaxial tests in compression and could be assessed using the following proposed equation [7]:

$$\varepsilon_{\text{acc}} = f_{\text{ampl}} f_p f_Y f_e f_N f_\pi, \tag{3}$$

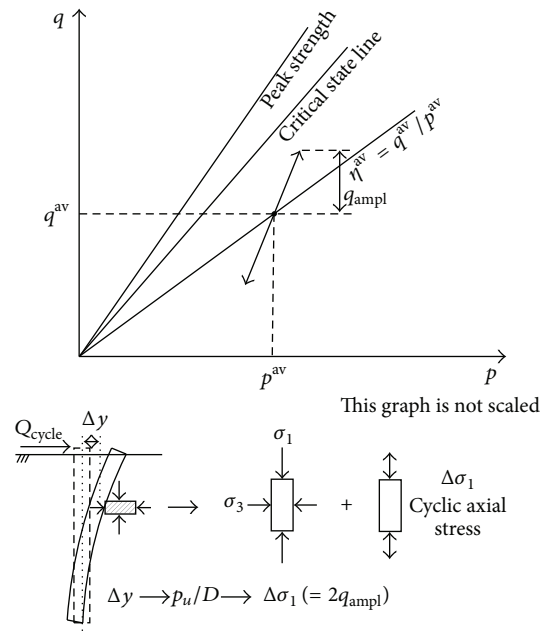

FIGURE 6: Stress path in p-q plane from a cyclic triaxial test in compression.

TABLE 1: Summary of the partial functions f_i and a list of the material constants C_i for the tested sand [7].

Function	Material constants	
$f_{\text{ampl}} = \left(\frac{\varepsilon^{\text{ampl}}}{\varepsilon^{\text{ampl}}_{\text{ref}}}\right)^2$	$\varepsilon^{\text{ampl}}_{\text{ref}}$	10^{-4}
$f_N = C_{N1}[\ln(1 + C_{N2}N) + C_{N3}N]$	C_{N1}	3.4×10^{-4}
	C_{N2}	0.55
	C_{N3}	6.0×10^{-5}
$f_p = \exp\left[-C_p\left(\frac{p^{\text{av}}}{p_{\text{ref}}} - 1\right)\right]$	C_p	0.43
	p_{ref}	100 kPa
$f_y = \exp(C_Y \overline{Y^{\text{av}}})$	C_Y	2.0
$f_e = \frac{(C_e - e)^2}{1 + e} \frac{1 + e_{\text{ref}}}{(C_e - e_{\text{ref}})^2}$	C_e	0.54
	e_{ref}	0.874
$f_\pi = 1$, if polarization = constant		

where f_{ampl} is a coefficient for strain amplitude, f_p is a coefficient for average mean stress (p^{av}), f_Y is a coefficient for average stress ratio (Y^{av}), f_e is a coefficient for void ratio, f_N is a coefficient for number of cycles, and f_π is a factor associated with polarization change. Equation (3) was originally developed for the norm of the strain tensor, but within this paper the assumption is made for simplification that the total strain predicted by (3) equals the horizontal strain in the soil at the front of the pile. Table 1 summarizes the partial functions for the coefficients and the suggested material constants used in this study.

Figure 6 illustrates the stress path in the p-q plane applied in a cyclic triaxial test in compression. When cyclic lateral load is applied to the pile head, the soils at the pile front are compressed and released repeatedly, which can be

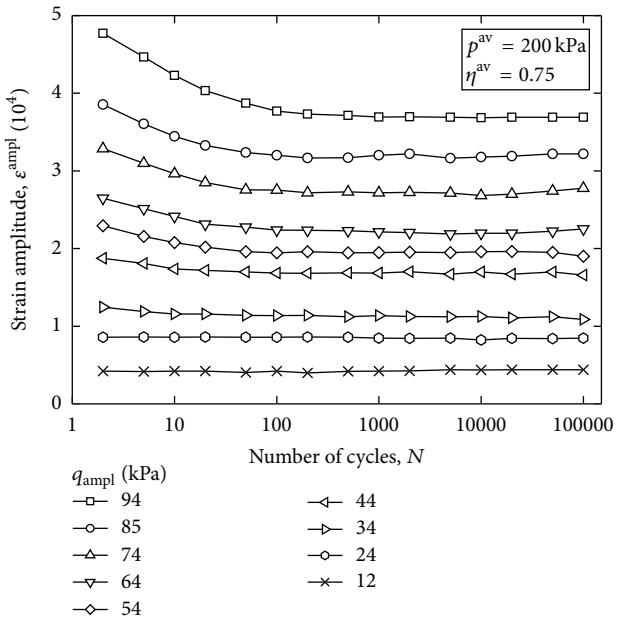

Figure 7: Development of strain amplitude with number of cycles for different deviatoric stress amplitudes (redrawn from [7]).

simulated by cyclic triaxial test in compression. In fact, the SWM recommends using triaxial compression test results [17]; thus the results from cyclic triaxial test in compression were adopted in this study. Increase in axial (horizontal) stress ($\Delta\sigma_1$) causes an increasing deviatoric stress from the initial in situ stress on the η^{av}– line to the desired deviatoric stress amplitude (q_{ampl}) above the η^{av}– line, and then the axial stress decreased causing a decrease in deviatoric stress to the desired amplitude under the η^{av}– line. In one way loading condition, the cyclic lateral load (Q_{cyc}) induces the deviatoric stress amplitude (q_{ampl}) above and under the η^{av}– line, indicating that the increase in the axial stress ($\Delta\sigma_1$) is twice the deviatoric stress amplitude. It should be noted that Ashour et al. [17] recommend using conventional triaxial compression test where the confining pressure is isotropic. However, the cyclic triaxial test has anisotropic confining pressure before applying cyclic axial stress. The anisotropic confining pressure as shown in the p-q plane is appropriate for in situ stress condition, and the cyclic lateral load induces axial stress always greater than zero which occurs in one way cyclic loading condition.

The coefficient for the amplitude (f_{ampl}) could be calculated from strain amplitude (ε^{ampl}) which decreased with the number of cycles in the cyclic triaxial tests with constant stress amplitude. Figure 7 shows the development of strain amplitude with the number of cycles for various deviatoric stress amplitudes at an average stress with p_{av} = 200 kPa and η^{av} = 0.75. In order to calculate deviatoric stress amplitude along the pile resulting from cyclic lateral load, SWM analyses were conducted using static strains. From the static analyses, the p-y curves and pile deflection curves were obtained. The p-y curves provide the soil resistance per unit length (p) at a specific lateral displacement (y), and the lateral displacement

Table 2: Strain amplitudes along the pile derived from Figure 7 for different lateral cyclic loads of the pile and different numbers of cycles (unit: 10^{-4}).

Depth (m)	ε_{ampl}					
	25% Q_u		50% Q_u		75% Q_u	
	$N = 1$	$N = 10^5$	$N = 1$	$N = 10^5$	$N = 1$	$N = 10^5$
5	2.08	2.05	4.16	3.67	5.49	4.55
15	1.87	1.63	3.49	2.97	5.11	4.27
25	0.84	0.83	2.00	1.77	2.68	2.28
35	0.30	0.31	0.97	0.85	2.01	1.67

Table 3: Calculated coefficients f_{ampl} for strain amplitude.

Depth (m)	f_{ampl}					
	25% Q_u		50% Q_u		75% Q_u	
	$N = 1$	$N = 10^5$	$N = 1$	$N = 10^5$	$N = 1$	$N = 10^5$
5	4.32	4.21	17.29	13.50	30.13	20.68
15	3.49	2.65	12.18	8.81	26.16	18.25
25	0.71	0.69	4.00	3.12	7.20	5.21
35	0.09	0.10	0.94	0.72	4.06	2.78

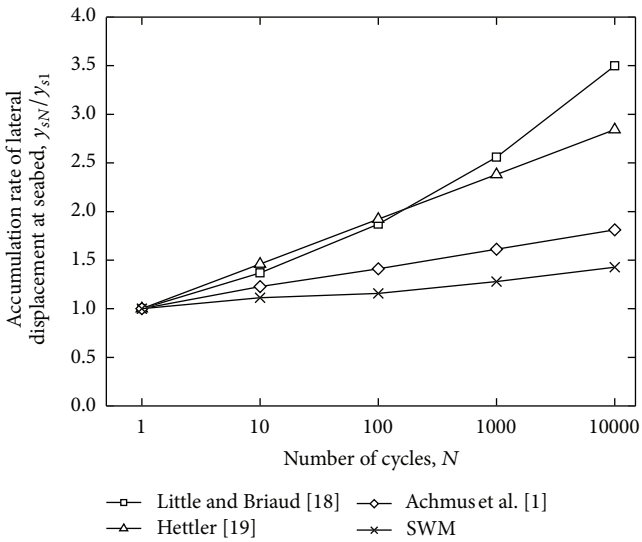

Figure 8: Comparison of accumulation rates of monopile displacement at seabed.

can be obtained from pile deflection curves. The estimated soil resistance per unit length was divided by the pile diameter (7.5 m), resulting in the increase in cyclic axial stress ($\Delta\sigma_1$). The deviatoric stress amplitude is half the cyclic axial stress. In the same way, the deviatoric stress amplitudes along the pile at 5, 15, 25, and 35 m depth were obtained.

Using the obtained deviatoric stress amplitudes along the pile, the strain amplitudes were estimated using Figure 7. Linear interpolation technique was used when exact deviatoric stress amplitude is unavailable. As the strain amplitude was measured with an average mean pressure of 200 kPa, the strain amplitude needs correction to account for the effect of pressure dependency of the secant stiffness. With simple

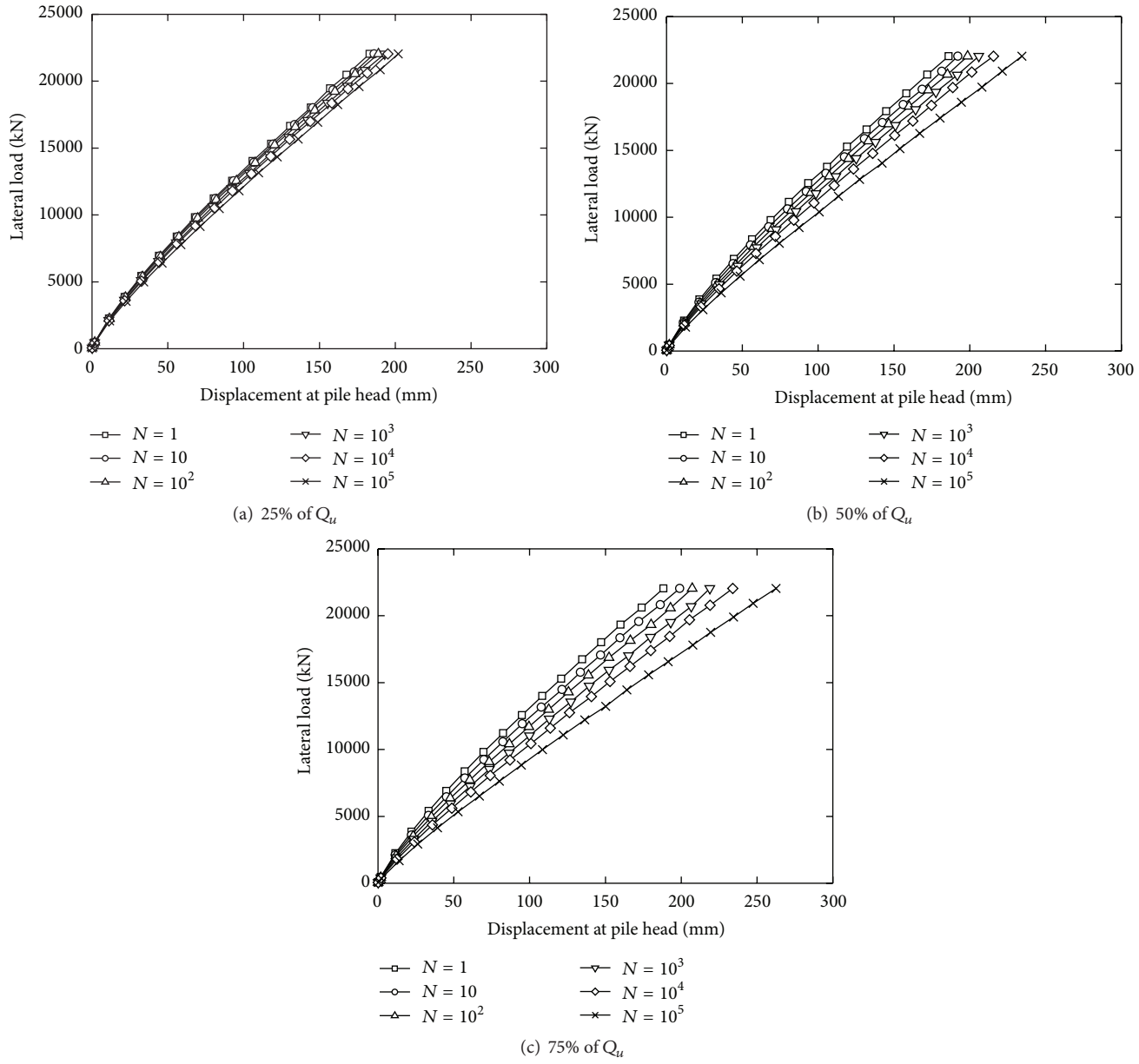

Figure 9: Load-displacement curves at pile head for 3 cyclic lateral loads: (a) 25%, (b) 50%, and (c) 75% of the static capacity (Q_u).

Table 4: Calculated coefficients for number of cycles, average stress ratio, void ratio, polarization changes, and average mean stress.

Depth (m)	p^{av} (kPa)	q^{av} (kPa)	η^{av}	Coefficient								
				f_N (10^{-4})					f_Y	f_e	f_π	f_p
				$N = 1$	$N = 10^2$	$N = 10^3$	$N = 10^4$	$N = 10^5$				
5	36.67	27.50	0.75	1.49	6.37	13.71	21.66	57.51	1.53	0.13	1	1.40
15	110.00	82.50										0.96
25	183.33	137.50										0.70
35	256.67	192.50										0.51
				Independent of depth					Constant values were used			Independent of N

Table 5: Accumulated strains and input strains at $N = 1$ and $N = 10^5$ (unit: 10^{-4}).

Depth (m)	25% Q_u				50% Q_u				75% Q_u			
	$\varepsilon_{\text{acc},N=\text{cyc}}$		$\varepsilon_{50,N=\text{cyc}}$		$\varepsilon_{\text{acc},N=\text{cyc}}$		$\varepsilon_{50,N=\text{cyc}}$		$\varepsilon_{\text{acc},N=\text{cyc}}$		$\varepsilon_{50,N=\text{cyc}}$	
	$N = 1$	$N = 10^5$	$N = 1$	$N = 10^5$	$N = 1$	$N = 10^5$	$N = 1$	$N = 10^5$	$N = 1$	$N = 10^5$	$N = 1$	$N = 10^5$
5	0.17	6.52	4.59	10.93	0.69	20.90	5.11	25.31	1.21	32.02	5.62	36.43
15	0.10	2.81	5.59	8.31	0.33	9.35	5.83	14.84	0.72	19.36	6.21	24.85
25	0.01	0.54	6.10	6.62	0.08	2.42	6.17	8.50	0.14	4.03	6.23	10.12
35	0.00	0.05	6.51	6.57	0.01	0.40	6.52	6.91	0.06	1.57	6.57	8.08

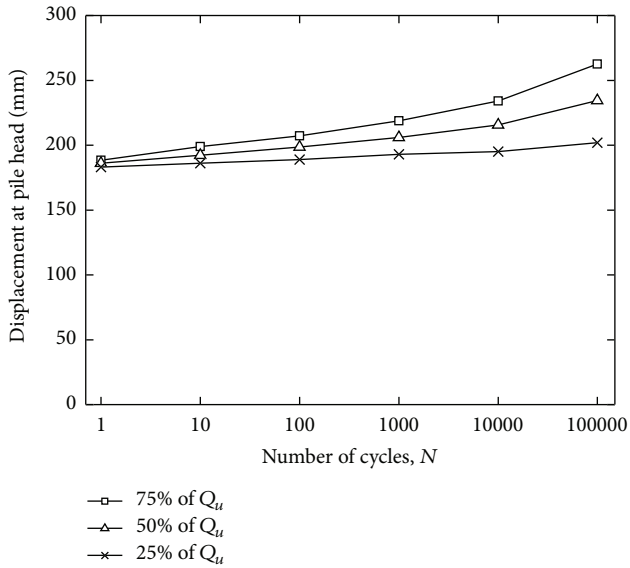

Figure 10: Effect of number of cycles on the displacement at pile head.

assumption that Young's modulus is proportional to the square root of average mean stress (4), the strain amplitudes at different mean stresses (different depth) were calculated. Using the correction factor, c_p, provided in (5), the strain amplitudes for every mean stress were calculated as shown in (6). Applying the correction factors to the strain amplitudes, the pressure dependency of strain amplitudes was considered along the pile.

Table 2 provides the strain amplitudes for different depths and number of cycles (1 and 10^5) under 3 cyclic lateral loads. The cyclic lateral loads were selected at 25%, 50%, and 75% of the static capacity. As shown in the table, the strain amplitudes were found to be larger for higher cyclic lateral loads, implying that the largest cyclic lateral load (75% of the static capacity) would lead to the largest accumulated strains, and consequently to the largest lateral displacement:

$$E \propto \left(p^{\text{av}}\right)^{0.5}, \tag{4}$$

$$c_p = \sqrt{\frac{p^{\text{av}}_{\text{ref}}\ (= 200\,\text{kPa})}{p^{\text{av}}}}, \tag{5}$$

$$\varepsilon^{\text{ampl}}_{p^{\text{av}}} = c_p \varepsilon^{\text{ampl}}_{p^{\text{av}}_{\text{ref}}}. \tag{6}$$

The coefficient for the number of cycles (f_N) was simply calculated by inserting the number of cycles under consideration together with the suggested material constants into the partial function provided in Table 1. It was reported that the accumulated strain increased with decreasing average mean stress, and the coefficient for average mean stress (f_p) was slightly affected by the number of cycles [7]. However, the recommended material constants neglected the effect of the number of cycles and were adopted as such in this study. The average stress ratio (the ratio of the average deviatoric stress to the average mean stress) as well as the void ratio was assumed to be constant; accordingly, the coefficients, f_Y and f_e, were calculated to be 1.53 and 0.13. The coefficient f_π was 1.0 since polarization changes were not considered in this study.

Tables 3 and 4 present the calculated coefficients for the influences of the strain amplitude, number of cycles, average stress ratio, void ratio, polarization, and average mean stress. The homogeneous subground was divided into 10 m thick layers, and the coefficients were calculated for each layer. It is shown that the coefficients f_{ampl} for strain amplitude significantly vary with depths but only slightly with the number of cycles and that the coefficients f_N for the number of cycles vary from 1.49 (10^{-4}) to 57.51 (10^{-4}) for 1 and 10^5 cycles, respectively. Table 5 tabulates the calculated accumulated strains and input strains at $N = 1$ and 10^5 accounting for all the coefficients provided in Tables 3 and 4. It is clearly shown that most accumulated strains develop at a depth shallower than 25 m regardless of the number of cycles. This agrees well with the fact that the strain amplitudes are very small at the greater depths for the given cyclic lateral loads. The magnitude of input strains is found to be larger for larger cyclic lateral loads and larger numbers of cycles.

4. Numerical Results and Discussion

4.1. SWM Analysis versus FEM. Achmus et al. [1] performed the Finite Element Method (FEM) with the stiffness degradation model to investigate the accumulated displacement due to cyclic loading. In order to check the applicability of the SWM analysis for cyclic lateral loading, the lateral displacement of pile at seabed level was compared with the FEM results (Figure 8). The used soil and pile properties are identical to those in Figure 1, and the used cyclic lateral load was 15.0 MN. The number of cycles ranges from 1 to 10^4. It is shown that the displacement at seabed is similar for both analyses when $N = 1$, but the SWM analysis tends to underestimate the displacement when the number of cycles

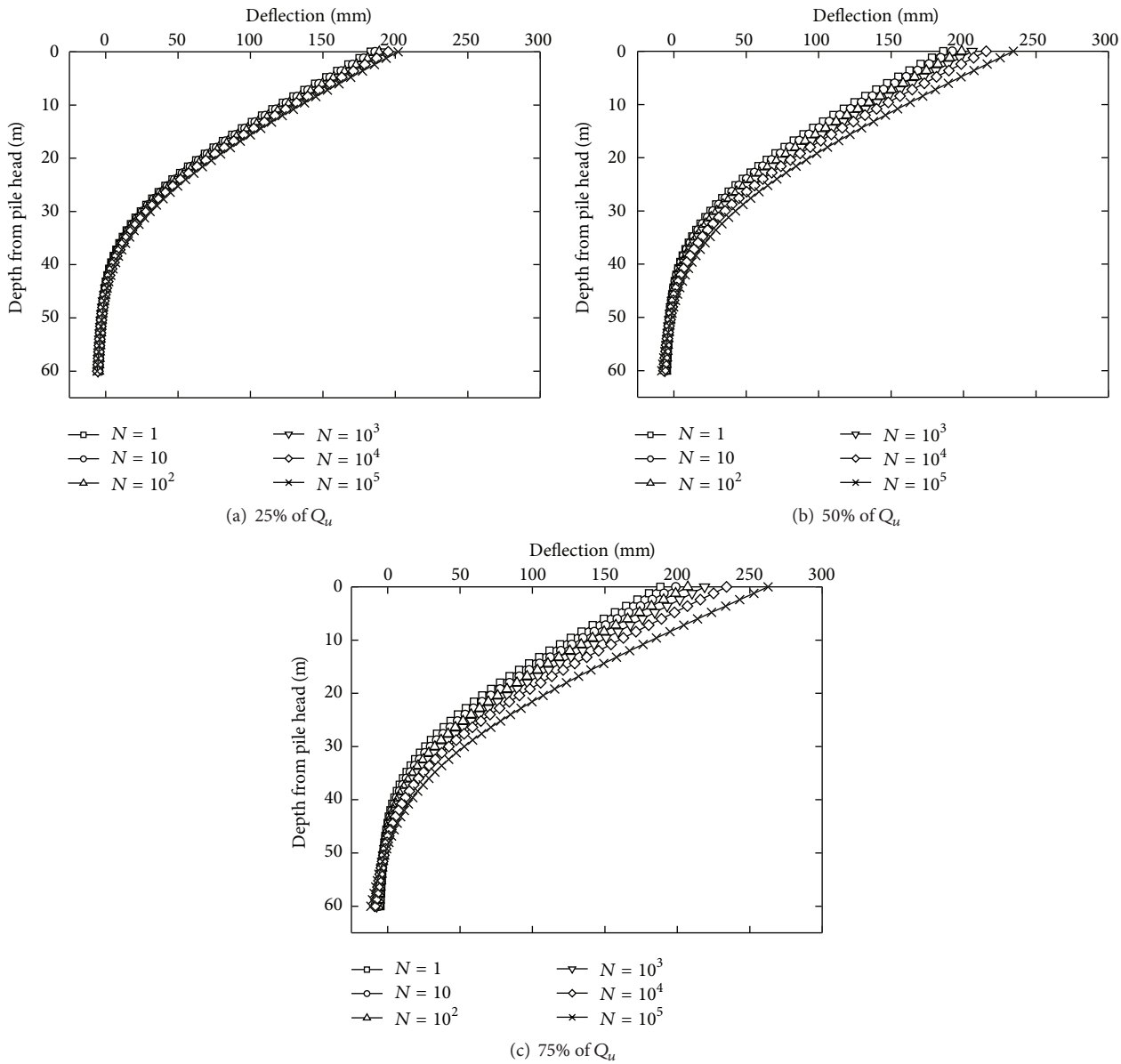

Figure 11: Pile deflection curves for 3 cyclic lateral loads: (a) 25%, (b) 50%, and (c) 75% of the static capacity (Q_u).

gets higher. For $N = 10^4$, the SWM analysis predicts 46% increase in lateral displacement whereas the FEM predicts 80% increase. Both FEM and SWM analyses predict the increase in accumulated lateral displacement with increasing number of cycles but underestimate the displacements compared to the predictions proposed by other researchers [18, 19].

4.2. Load-Displacement Curve. Figure 9 shows the load-displacement curves at the pile head for different cyclic lateral loads and numbers of cycles. For the given lateral load of 22.04 MN, the pile was found to be more displaced as the number of cycles increased. When cyclic lateral load was assumed to be 25% of the static capacity, the displacement for 1 cycle of lateral load was 183.11 mm but increased up to 201.93 mm for 10^5 cycles. The 10^5 cycles are likely to induce approximately 111% additional displacement for the same magnitude of lateral load (22.04 MN). The discrepancy between the displacements at $N = 1$ and 10^5 appeared to significantly grow when the largest magnitude in cyclic lateral load was considered (75% of the static capacity). With the largest cyclic load, the lateral displacement for 10^5 cycles was calculated to be approximately 140% of the displacement under static loading. It was found that an increase both in the magnitude of the cyclic lateral load and in the number of cycles significantly increases the accumulated lateral displacement.

Figure 10 summarizes the effect of the number of cycles and the cyclic lateral load on the lateral displacement at pile head. The lateral displacement appeared to increase

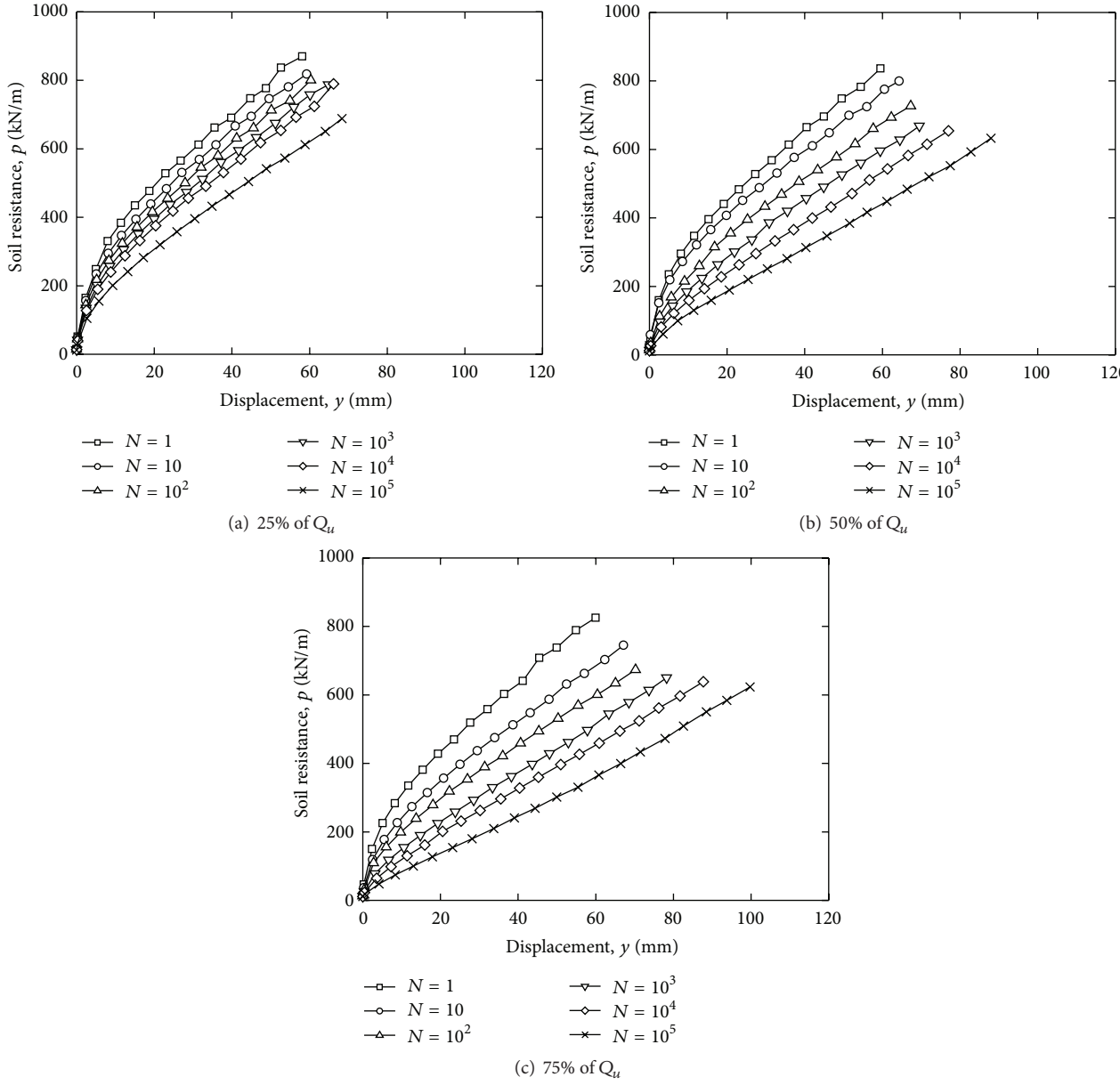

Figure 12: p-y curves at 2 m depth for 3 cyclic loads: (a) 25%, (b) 50%, and (c) 75% of the static capacity (Q_u).

exponentially with increasing logarithm of the number of cycles, leading to about 40% increase of the displacement when comparing $N = 1$ with $N = 10^5$ cycles. This implies that the lateral displacement properly predicted for static lateral load would be inappropriate for cyclic loading conditions. It should be noted that the partial safety factor for displacement is usually 1.0 in offshore pile design.

4.3. Pile Deflection Curve. Figure 11 presents deflection curves along the pile. Similar to the load-displacement curves, the pile deflection increased with increasing number of cycles and growing cyclic lateral load. Even though the pile does not deflect significantly below 30 m depth, the deflection near the ground surface considerably differs depending on loading conditions. For the smallest cyclic lateral load, the pile deflections calculated for the various numbers of cycles did not significantly differ; however, the deflection was clearly dependent on the number of cycles for the biggest lateral load.

4.4. Cyclic p-y Curves. Figures 12-13 present p-y curves at 2 and 4 m depth considering the effect of cyclic loading, indicating that the consideration of the cumulative deformations due to cyclic loading leads to a considerable decrease of the initial stiffness of the p-y curves. Even though SWM provides p-y curves at any desired locations, two shallow depths were particularly chosen because soil properties near the ground surface play a key role in the lateral behavior of the monopile. As shown in the figures, the initial stiffness of

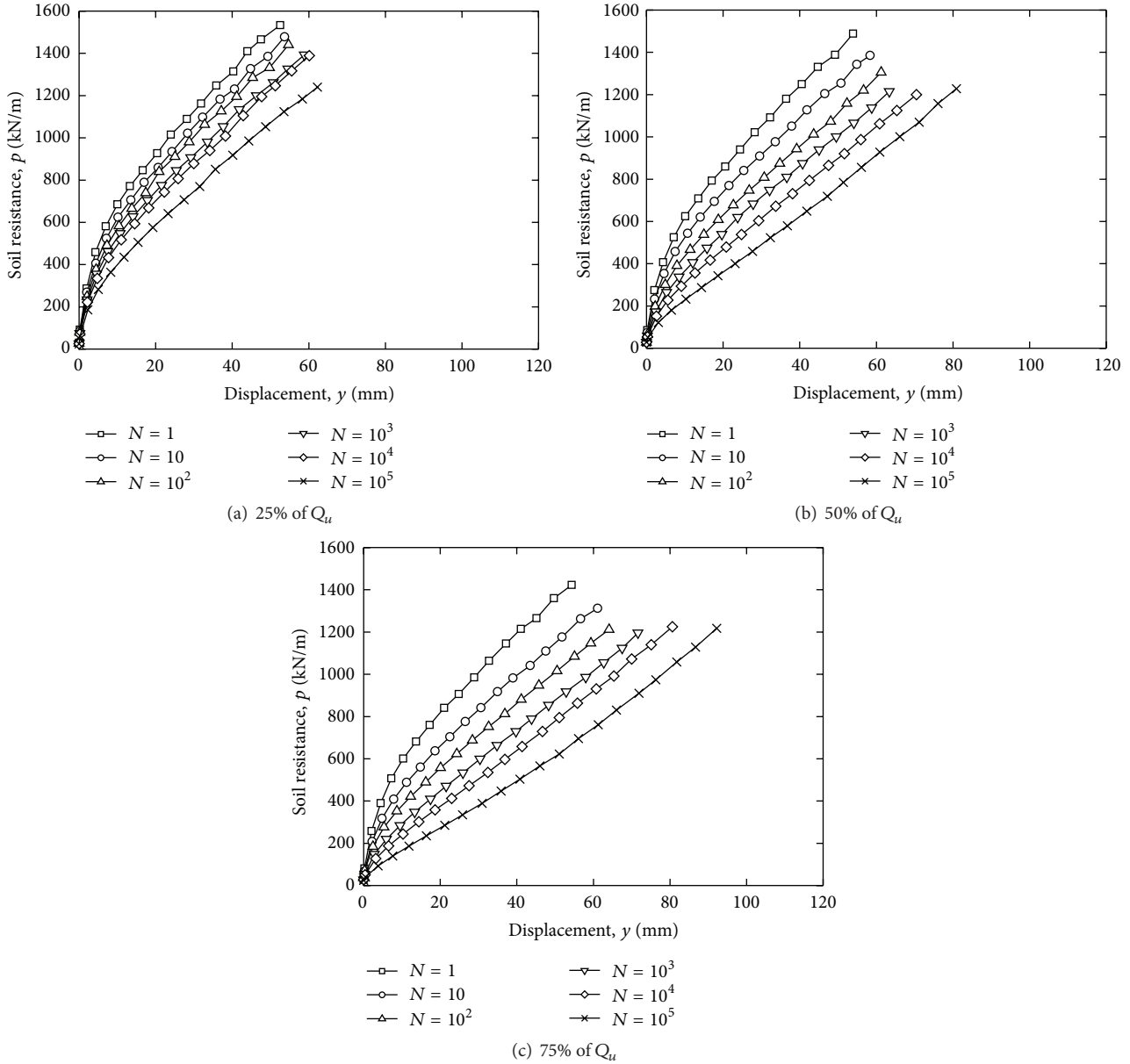

Figure 13: p-y curves at 4 m depth for 3 cyclic loads: (a) 25%, (b) 50%, and (c) 75% of the static capacity (Q_u).

the p-y curves sharply decreased with increasing number of cycles and increasing cyclic lateral load. The stiffness decrease becomes more prominent with increasing cyclic lateral load. Such trends in the p-y curves do not differ with depth.

5. Conclusions

In this study, the lateral behavior of a monopile for an offshore wind turbine subject to cyclic loading was investigated using the SWM analysis in combination with the data from drained cyclic triaxial compression test results on quartz sand. From the SWM analyses, the load-displacement curves, deflection curves, and p-y curves were obtained and compared with each other. The following conclusions were drawn:

(1) A new approach was proposed to investigate the effect of cyclic lateral loads on the lateral behavior of monopiles. The approach employed the input strains ($\varepsilon_{50,N=\text{cyc}}$), which were calculated based on the accumulated strains caused by cyclic lateral loads ($\varepsilon_{\text{acc},N=\text{cyc}}$) and the static strains ($\varepsilon_{50,\text{static}}$).

(2) The displacement at pile head, representing the sum of accumulated displacements due to a cyclic loading and a subsequent monotonic loading towards a maximum load larger than the amplitude of the cycles, was found to increase exponentially as the logarithm of the number of cycles increased. For a given lateral load of 22.04 MN (lateral static capacity of the pile under consideration), the increase in lateral

displacement at pile head was 111% if 10^5 cycles with an amplitude corresponding to 25% of the static capacity had been previously applied. The increase of the lateral displacement due to preceding cycles becomes as much as 140% at an amplitude corresponding to 75% of the static capacity.

(3) The p-y curves obtained at 2 and 4 m depths indicated that the initial stiffness of the p-y curves considerably decreased with increasing number of cycles. The decrease became prominent when the cyclic lateral load was 75% of the static capacity. However, it should be kept in mind that this decrease of stiffness is some kind of "calculation" in order to consider the accumulated deformations. The real stiffness of the sand surrounding the pile usually increases due to compaction.

(4) The application of existing p-y curves without considering cyclic loading would lead to an underestimation of the lateral displacement at pile head. Modified p-y curves accounting for the magnitude of cyclic loading and number of cycles are required to be used in the BEF analysis.

Conflict of Interests

The authors declare that there is no conflict of interests regarding the publication of this paper.

Acknowledgments

This work was partially supported by National Research Foundation of Korea (NRF) funded by Ministry of Science, ICT & Future Planning (NRF-2013R1A1A1011983), and Korea Institute of Ocean Science and Technology (20113010020010-11-3-510).

References

[1] M. Achmus, Y.-S. Kuo, and K. Abdel-Rahman, "Behavior of monopile foundations under cyclic lateral load," *Computers and Geotechnics*, vol. 36, no. 5, pp. 725–735, 2009.

[2] E. Winkler, *Theory of Elasticity and Strength*, Domimicus, Prague, Czech Republic, 1867.

[3] L. C. Reese, W. R. Cox, and F. D. Koop, "Analysis of laterally loaded piles in sand," in *Proceedings of the Offshore Technology in Civil Engineering: sHall of Fame Papers from the Early Years*, pp. 95–105, Houston, Tex, USA, May 1974.

[4] D. Bogard and H. Matlock, "Simplified calculation of p-y curves for laterally loaded piles in sand," Tech. Rep., The Earth Technology, Houston, Tex, USA, 1980.

[5] T. Wichtmann, A. Niemunis, and T. Triantafyllidis, "Prediction of long-term deformations for monopile foundations of offshore wind power plants," in *Proceedings of the 11th Baltic Sea Geotechnical Conference: Geotechnics in Maritime Engineering*, Gdańsk, Poland, September 2008.

[6] T. Wichtmann, A. Niemunis, and T. Triantafyllidis, "Towards the FE prediction of permanent deformations of offshore wind power plant foundations using a high-cycle accumulation model," in *Proceedings of the 2nd International Symposium on Frontiers in Offshore Geotechnics (ISFOG '10)*, pp. 635–640, November 2010.

[7] T. Wichtmann, A. Niemunis, and T. Triantafyllidis, "Strain accumulation in sand due to cyclic loading: drained triaxial tests," *Soil Dynamics and Earthquake Engineering*, vol. 25, no. 12, pp. 967–979, 2005.

[8] T. Wichtmann, A. Niemunis, and T. Triantafyllidis, "Strain accumulation in sand due to cyclic loading: drained cyclic tests with triaxial extension," *Soil Dynamics and Earthquake Engineering*, vol. 27, no. 1, pp. 42–48, 2007.

[9] P. Hinz, K. Lesny, and W. Richwien, "Prediction of monopile deformation under high cyclic lateral loading," in *Proceedings of the 8th German Wind Energy Conference*, DEWEK, Bremen, Germany, 2006.

[10] M. Heidari, M. Jahanandish, H. E. Naggar, and A. Ghahramani, "Nonlinear cyclic behavior of laterally loaded pile in cohesive soil," *Canadian Geotechnical Journal*, vol. 51, no. 2, pp. 129–143, 2014.

[11] H. R. Roesen, L. B. Ibsen, and L. V. Andersen, "Experimental testing of monopiles in sand subjected to one-way long-term cyclic lateral loading," in *Proceedings of the 18th International Conference on Soil Mechanics and Geotechnical Engineering*, 2013.

[12] H. R. Roesen, L. B. Ibsen, M. Hansen, T. K. Wolf, and K. L. Rasmussen, "Laboratory testing of cyclic laterally loaded pile in cohesionless soil," in *Proceedings of the 23rd International Offshore and Polar Engineering Conference (ISOPE '13)*, pp. 594–601, July 2013.

[13] I. F. Moller and T. H. Christiansen, *Laterally loaded monopile in dry and saturated sand—static and cyclic loading [M.S. thesis]*, Aalborg University, Aalborg, Denmark, 2011.

[14] L. C. C. Geopile, "SWM 6.2 version 6.2 : Laterally and axially loaded single pile and pile group," 2000.

[15] AASHTO, *AASHTO LRFD Bridge Design Specifications*, American Association of Highway and Transportation Officials, Washington, DC, USA, 2007.

[16] G. Norris, "Theoretically based BEF laterally loaded pile analysis," in *Proceedings of the 3rd International Conference on Numerical Methods in Offshore Piling*, pp. 361–386, Nantes, France, 1986.

[17] M. Ashour, G. Norris, and P. Pilling, "Lateral loading of a pile in layered soil using the strain wedge model," *Journal of Geotechnical and Geoenvironmental Engineering*, vol. 124, no. 4, pp. 303–314, 1998.

[18] R. L. Little and J. L. Briaud, "Full scale cyclic lateral load tests on six single piles in sand," Miscellaneous Paper GL-88-27, Geotechnical Division, Texas A&M Unuiversity, College Station, Tex, USA, 1988.

[19] A. Hettler, *Verschiebungen Starrer und Elastischer Gründungskörper in Sand bei Monotoner und Zyklischer Belastung*, Institut für Bodenmechanik und Felsmechanik der Universität Fridericiana, Karlsruhe, Germany, 1981.